(Received 11 December 2024, Accepted 28 January 2025, Scheduled 7 February 2025)

Emergence of Diffractive Phenomena in Finite Arrays of Subwavelength Scatterers

Ilya Karavaev[1, 2], Ravshanjon Nazarov[2], Yicheng Li[2], Andrey A. Bogdanov[1, 2, *], and Denis G. Baranov[1, 3, *]

[1] *Qingdao Innovation and Development Center of Harbin Engineering University, Qingdao 266000, Shandong, China*
[2] *ITMO University, St. Petersburg 197101, Russia*
[3] *Center for Photonics and 2D Materials, Moscow Institute of Physics and Technology, Dolgoprudny 141700, Russia*

ABSTRACT: Periodic optical structures, such as diffraction gratings and numerous photonic crystals, are one of the staples of modern nanophotonics for the manipulation of electromagnetic radiation. The array of subwavelength dielectric rods is one of the simplest platforms, which, despite its simplicity exhibits extraordinary wave phenomena, such as diffraction anomalies and narrow reflective resonances. Despite the well-documented properties of infinite periodic systems, the behavior of these diffractive effects in systems incorporating a finite number of elements is studied to a far lesser extent. Here we theoretically and numerically study the evolution of collective spectral features in finite arrays of dielectric rods. We develop an analytical model of light scattering by a finite array of circular rods based on the coupled dipoles approximation and analyze the spectral features of finite arrays within the developed model. Finally, we validate the results of the analytical model using full-wave numerical simulations.

1. INTRODUCTION

Periodic optical structures, such as diffraction grating, various photonic crystals, wire metamaterials, offer a wide range of optical phenomena, such as optical band gaps, hyperbolic dispersion, negative refraction, subwavelength imaging, and others [1–5]. This diversity of possible optical behaviors, studied since the pioneering works of Wood and Rayleigh [6, 7], makes periodic optical structures one of the staples of modern nanophotonics for advanced light manipulation [8, 9]. Ultimately, the resonances of such arrays enable optical bound states in the continuum (BIC) [10–12]. In real structures BICs can be detected as resonant states with sufficiently high quality factors [13, 14]. The theoretical and experimental investigations of the BICs have opened up novel avenues in the study of topologically protected states [15], creation of lasers [16] and highly sensitive dielectric sensors [17].

Particularly, periodic arrays of dielectric rods present an ultimately simple optical system that, nevertheless, is capable of exhibiting some extraordinary wave phenomena [18, 19]. Previous theoretical and experimental studies have shown remarkable spectral features in arrays of thin dielectric rods, such as ultra-narrow resonances and total transmission [18, 20–22]. These effects have been attributed to the far-field inter-particle interactions in the system in the vicinity of so called diffraction, or Rayleigh, anomalies [1]. Interestingly, total transmission in an array of thin rods occurring exactly at the Rayleigh anomaly remains even in the presence of material losses in the dielectric rods. Although these and related effects have been widely studied and verified experimentally [23] in periodic structures, one can wonder how these diffractive effects emerge in finite systems incorporating only a finite number of scattering elements.

Besides infinite truly periodic arrays, optical properties of *finite* arrays have also been studied to some extent. Evlyukhin et al. studied the response of finite two-dimensional arrays of resonant dielectric and metallic particles [24, 25]. Several groups have studied the size effect on the response of finite 2D arrays [26–29] and showed that the optical properties of a finite array gradually approach that of the infinite one. Some also studied the effect of size and disorder on resonances of plasmonic 2D arrays in the context of lasing modes [30–32]. More recent research efforts explored the size-effect in 2D arrays of resonant dielectric particles in the context of the collective Kerker effect [33] and the formation of high-Q quasi-BIC states in finite-size metasurfaces [34] and atomic arrays [35, 36]. These theoretical results have also been accompanied by an impressive experimental progress in realization of reflective finite atomic arrays [37].

Several works have also analyzed the size-effects in 1D arrays of thin wires [38, 39] and nanostrips [40] with emphasis on the behavior of the resonances. Others analyzed the spectral properties of finite and semi-infinite chains of subwavelength particles [41–44], as well as the transmission properties of in finite chains of subwavelength dielectric resonators [45], and the formation of high-Q resonances in such chains [46]. However, very little work has been accomplished to analyze the effect of the array size on the Rayleigh anomalies, occurring at the onset of new diffraction orders, with only some theoretical efforts devoted to studies of excitation of a finite one-dimensional chain at the Rayleigh anomaly [47].

* Corresponding authors: Andrey A. Bogdanov (bogdan.taurus@gmail.com); Denis G. Baranov (baranov.mipt@gmail.com).

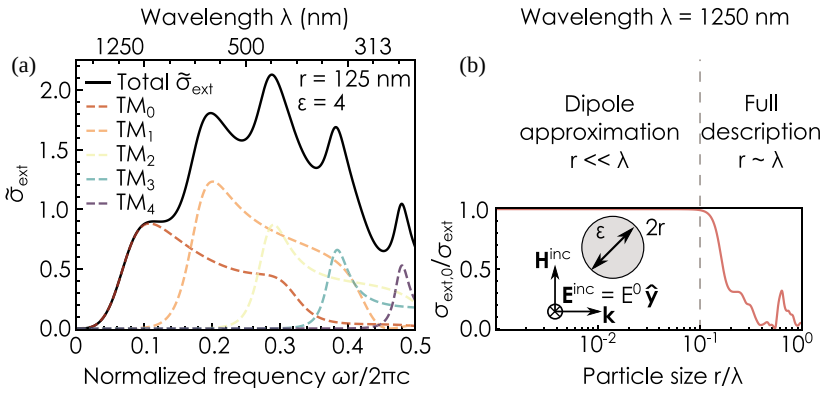

FIGURE 1. (a) Exact analytical solution for scattering cross-section spectra of an individual dielectric circular cylinder with permittivity $\varepsilon = 4$ and $r = 125\,\text{nm}$ under TM-polarized illumination. (b) Monopole $\ell = 0$ TM harmonic contribution to the total extinction cross-section under TM-polarized illumination at the wavelength $\lambda = 500\,\text{nm}$ as the function of particle radius r.

In this paper, we theoretically investigate the evolution of collective spectral features in finite arrays of dielectric rods supporting both narrow optical resonances, as well as Rayleigh anomalies. Based on the existing coupled dipoles approximation (CDA) model, we analytically solve the problem of light scattering by a finite array of circular rods. Using this model, we examine the effect of the number of the elements of a finite array and the material absorption on the extinction spectra of the array. Using the very same analytical model, we study the eigenfrequencies distribution as a function of the number of the elements. Next, we verify the results of the CDA-based analytical model by performing numerical simulations of the finite system. Finally, we examine the effect of the rod cross-section and the presence of a substrate on these phenomena.

The rest of the paper is organized as follows. in Section 2, we present the optical properties (cross-section and polarizabilities) of an individual dielectric rod. In Section 3, we present the theory of light scattering by an infinite periodic array from [20] and reproduce the key spectral features of the system under TM illumination (electric field along the cylinder axis). In Section 4, we study mentioned spectral features in a finite array of both dielectric and metallic rods and study the effect of the material absorption on these spectral features. In Section 5, we compare the results of the theoretical model with the results of numerical simulations, and in Section 6, we analyze the effect of the rod cross-section and the presence of a substrate on the diffractive optical features of infinite arrays.

2. INDIVIDUAL ROD

We begin with a brief analysis of plane wave scattering by a single dielectric rod. Fig. 1(a) shows scattering cross-section of a single dielectric rod (refractive index $n = \sqrt{\varepsilon}$) in air illuminated with a normally-incident TM-polarized (magnetic field perpendicular to the axis) plane wave, as well as the partial multipole contributions of different cylindrical harmonics to the total cross-section.

For small size parameters $nk_0r \ll 1$ the cross-section is clearly dominated by the TM_0 monopole harmonic [see Fig. 1(b)]. In 3D space the zero order harmonic TM_0 produces the field of an infinitely extended electric dipole. This motivates further analysis of the optical response of a cylinder in dipole approximation and an introduction of the polarizability tensor of a single subwavelength cylinder in the following form

$$\overleftrightarrow{\alpha} = \text{diag}(\alpha_{xx}, \alpha_{yy}, \alpha_{zz}) \tag{1}$$

with $\alpha_{xx} = \alpha_{zz} = \text{i}\frac{8}{k_0^2}a_1$, and $\alpha_{yy} = \text{i}\frac{4}{k_0^2}b_0$. The dimensionless scattering coefficients a_1 and b_0 can be found in [48, p. 301]:

$$\begin{aligned} b_0 &= \frac{\sqrt{\varepsilon}J_0'(\sqrt{\varepsilon}k_0r)J_0(k_0r) - J_0(\sqrt{\varepsilon}k_0r)J_0'(k_0r)}{\sqrt{\varepsilon}J_0'(\sqrt{\varepsilon}k_0r)H_0^{(1)}(k_0r) - J_0(\sqrt{\varepsilon}k_0r)H_0^{(1)'}(k_0r)}, \\ a_1 &= \frac{J_1'(\sqrt{\varepsilon}k_0r)J_1(k_0r) - \sqrt{\varepsilon}J_1(\sqrt{\varepsilon}k_0r)J_1'(k_0r)}{J_1'(\sqrt{\varepsilon}k_0r)H_1^{(1)}(k_0r) - \sqrt{\varepsilon}J_1(\sqrt{\varepsilon}k_0r)H_1^{(1)'}(k_0r)}, \end{aligned} \tag{2}$$

where J_ℓ and $H_\ell^{(1)}$ are the Bessel and Hankel functions of the first kind of ℓth order, respectively, and $k_0 = \omega/c$ is the vacuum wavenumber.

3. INFINITE ARRAY

Next we analyze the spectral features of an infinite array. Fig. 1(a) illustrates the system under study. We consider a system of N parallel infinitely long circular dielectric cylinders in air with permittivity ε, radius r, and distance L between the centers of two neighboring rods. Let the array be illuminated with a linearly TM-polarized (electric field along the cylinders axes) plane wave:

$$\mathbf{E}^{\text{inc}}(\mathbf{r}) = \mathcal{E}\hat{\mathbf{y}}e^{ik_z z + ik_\parallel x} \tag{3}$$

with $k_z^2 + k_\parallel^2 = k^2$, $k = \omega/c$.

The total field is the sum of the background field and that radiated by the cylinders:

$$\mathbf{E}^{\text{tot}}(\mathbf{r}) = \mathbf{E}^{\text{inc}}(\mathbf{r}) + 4\pi k_0^2 \sum_j \overleftrightarrow{\mathbf{G}}(\mathbf{r}, \mathbf{r}_j)\mathbf{P}_j, \tag{4}$$

where $\mathbf{P}_j$ is the dipole moment of the jth scatterer defined by self-consistent exciting field, and $\overleftrightarrow{\mathbf{G}}$ is the free space dyadic

Green's function of the 2D Helmholtz equation:

$$\overleftrightarrow{\mathbf{G}}(\mathbf{r},\mathbf{r}') = \left(\mathbb{I}_{3\times3} + \frac{1}{k_0^2}\nabla\otimes\nabla\right)\frac{i}{4}H_0^{(1)}\left(k_0|\mathbf{r}-\mathbf{r}'|\right), \quad (5)$$

where $\mathbb{I}_{3\times3} = \mathrm{diag}(1,1,1)$ is the 3×3 identity matrix. The resulting Green's dyad is written in a compact form containing the in-plane as well as out of plane responses simultaneously. For TM polarization, analyzed in the following, the scalar Green's function of Helmholtz equation in 2D is:

$$G(\mathbf{r},\mathbf{r}') = \frac{i}{4}H_0^{(1)}(k_0|\mathbf{r}-\mathbf{r}'|). \quad (6)$$

For incident TM polarization, electric dipole induced in jth cylinder is related to the total field via the yy-component of the bare polarizability tensor, Eq. (1):

$$\mathbf{P}_j \equiv \mathbf{P}(\mathbf{r}_j) = \alpha_{yy}\mathbf{E}^{\mathrm{tot}}(\mathbf{r}_j). \quad (7)$$

The total field acting on the jth cylinder takes the form:

$$\mathbf{E}^{\mathrm{tot}}(\mathbf{r}_j) = \mathbf{E}^{\mathrm{inc}}(\mathbf{r}_j) + 4\pi k_0^2 G_{\mathrm{latt}}(k_\parallel)\mathbf{P}_j, \quad (8)$$

where the lattice sum G_{latt} accounts for the action of all other cylinders $i \neq j$ in the array [20]:

$$\begin{aligned} G_{\mathrm{latt}}(\omega,k_\parallel) &= i\left(\frac{1}{2Lk_z} - \frac{1}{4}\right) \\ &+ \frac{1}{2L}\sum_{m=1}^{\infty}\left(\frac{i}{k_z^{(m)}} + \frac{i}{k_z^{(-m)}} - \frac{L}{m\pi}\right) \\ &+ \frac{1}{2\pi}\left(\ln\frac{k_0 L}{4\pi} + \gamma_E\right), \end{aligned} \quad (9)$$

where

$$k_z^{(m)} = \sqrt{k_0^2 - q_m^2}, \quad q_m = k_\parallel + \frac{2\pi m}{L}, \quad (10)$$

are evaluated with radiation condition ($\mathfrak{Im}k_z^{(m)} > 0$), and γ_E is the Euler's constant.

With this at hand, we can express the induced dipole moments as:

$$\mathbf{P}_j = \tilde{\alpha}(\omega,k_\parallel)\mathbf{E}^{\mathrm{inc}}(\mathbf{r}_j), \quad (11)$$

where

$$\widetilde{\alpha}(\omega,k_\parallel) = \frac{1}{\alpha_{yy}^{-1} - 4\pi k_0^2 G_{\mathrm{latt}}} \quad (12)$$

is the renormalized (dressed) polarizability of the individual cylinder.

To calculate the total scattered field and present it as a Rayleigh series, we expand the Green's function over two-sided plane waves using Bessel identity:

$$H_0^{(1)}(kr) = \frac{1}{\pi}\int_{-\infty}^{+\infty} e^{ik_x x + ik_z|z|}\frac{dk_x}{k_z}. \quad (13)$$

The scattered field then takes the form of a set of diffraction orders:

$$\mathbf{E}^{\mathrm{scat}} = \mathcal{E}\hat{\mathbf{y}}\frac{i}{2L}\sum_m \frac{\widetilde{\alpha}}{k_z^{(m)}} e^{iq_m x + ik_z^{(m)}|z|}. \quad (14)$$

The orders with $\mathfrak{Re}k_z^{(m)} > 0, \mathfrak{Im}k_z^{(m)} = 0$ are the propagating ones, whiles the orders with $\mathfrak{Re}k_z^{(m)} = 0, \mathfrak{Im}k_z^{(m)} > 0$ are the evanescent ones, and do not contribute to the energy transfer away from the system. Finally, we obtain intensity reflection and transmission coefficients:

$$\mathcal{R} = \frac{1}{4L^2}\sum_{m_<}^{m_>}\frac{\left|4\pi k_0^2\widetilde{\alpha}\right|^2}{k_z^{(m)}k_z^{(0)}}, \quad (15)$$

$$\mathcal{T} = 1 - \frac{4\pi\mathfrak{Im}\widetilde{\alpha}}{Lk_z^{(0)}} + \frac{1}{4L^2}\sum_{m_<}^{m_>}\frac{\left|4\pi k_0^2\widetilde{\alpha}\right|^2}{k_z^{(m)}k_z^{(0)}}, \quad (16)$$

where

$$m_< = -\left\lfloor\frac{\omega/c + k_\parallel}{2\pi/L}\right\rfloor, \quad m_> = \left\lfloor\frac{\omega/c - k_\parallel}{2\pi/L}\right\rfloor \quad (17)$$

define the range of open (propagating) diffraction orders, and $\lfloor\ldots\rfloor$ denotes the floor operation. The first separate term in Eq. (16) describes the interference between the non-resonantly transmitted background field of the plane wave, and the field is radiated by the cylinders.

Since in a typical experimental setting higher-order diffracted signal is often not accessible with low-NA collection objectives, we will analyze pure specular zeroth-order reflection coefficient $\mathcal{R}_0$:

$$\mathcal{R}_0 = \frac{\left|4\pi k_0^2\widetilde{\alpha}\right|^2}{4k_z^{(0)2}L^2}. \quad (18)$$

Figure 2(b) presents specular intensity reflection spectra of an infinite array at normal incidence. The spectra clearly display two key features of the dielectric rods array. First, the array becomes transparent at the Rayleigh anomaly [18] defined by:

$$\frac{2\pi}{L}|m| = \frac{\omega}{c}, \quad m\in\mathbb{Z}, \quad (19)$$

corresponding to the opening of a new diffraction channel propagating along the array with $k_z^{(m)} = 0$ separating two qualitatively different cases labeled with numbers 1 and 2 at the right hand side of Fig. 2(a), which can be visualized with Ewald's sphere. The array becomes fully transparent at this point due to the divergence of the lattice sum [49]:

$$G_{\mathrm{latt}} \to \infty, \quad \mathcal{R} \to 0. \quad (20)$$

Oblique incidence lifts the degeneracy between ±1 diffraction orders and is expected to show qualitatively similar results at frequencies satisfying the following condition:

$$\left|k_\parallel + \frac{2\pi}{L}m\right| = \frac{\omega}{c}, \quad m\in\mathbb{Z}. \quad (21)$$

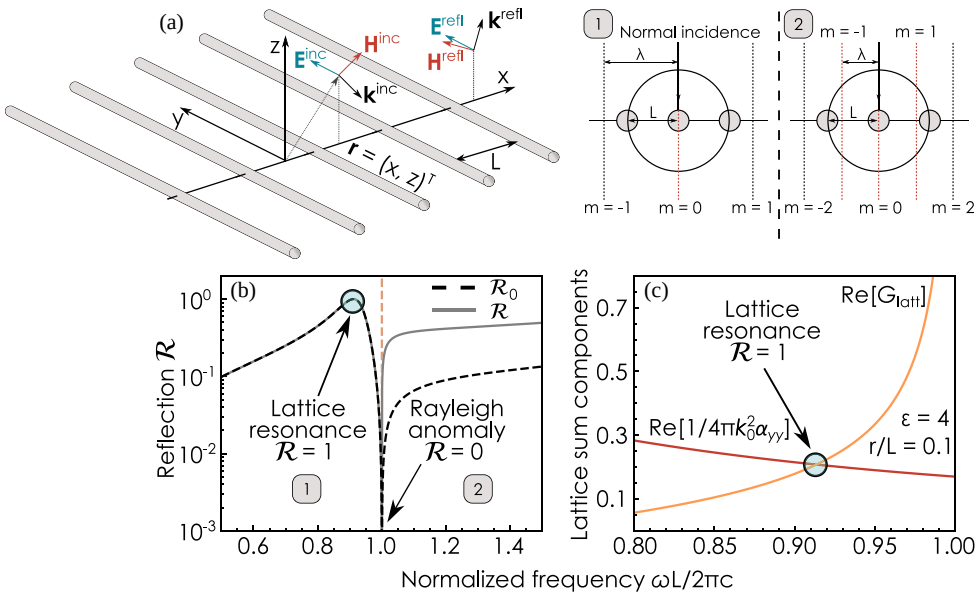

FIGURE 2. (a) Geometry of the system: an array of N parallel infinitely long circular cylinders with permittivity ε, radius r, and distance L between the centers of adjacent rods. (b) Specular $\Re_0$ (dashed) and total $\Re$ (solid) reflection spectra of an infinite periodic array of dielectric cylinders ($\varepsilon = 4$, $r = 0.1L$) under TM-polarized illumination at angle $\theta = 0$. The index inside the square denotes opened diffraction channels numbers. (c) Real part of the inverse dipole polarizability of a single cylinder, and that of the lattice sum as the function of frequency. Intersection of the curves corresponds to the total reflection condition $\Re = 1$.

In the following we limit our analysis to normal incidence.

Interestingly, the same structure would not show perfect transparency at the Rayleigh anomaly for TE incident polarization [18]. In this case, the response of each individual cylinder is quantified by two Cartesian components of the electric dipole moment P_x and P_z, and only one of them vanishes at the lattice singularity, while the other remains non-trivial and gives rise to non-zero scattered field, interfering with the background plane wave and in the end producing non-perfect transmission. For this reason, in the following we focus on TM polarization only.

Another interesting feature is observed at frequencies slightly below the first lattice singularity, where the array becomes fully reflective, $\mathcal{R} = \mathcal{R}_0 = 1$. These reflection peaks are a manifestation of the underlying quasi-normal modes of the array [19], which are solutions of the characteristic equation:

$$\widetilde{\alpha}^{-1}(\omega, k_{\|}) = 0. \tag{22}$$

For a fixed wave vector component $k_{\|}$ the solution of the characteristic equation defines a complex frequency at which the denominator of Eq. (12) vanishes [see Fig. 2(c)]. As a result, the above characteristic equation allows non-zero dipole moments in the infinite periodic array in the absence of incident field.

It is noteworthy that the specular reflection at the lattice resonance reaches exactly one [18]. This behavior can be well understood on the basis of the temporal coupled-mode theory [50, 51]. Indeed, below the onset of diffraction, the structure can be modeled as a single-mode cavity coupled radiatively to two scattering channels represented by oppositely propagating linearly-polarized plane waves. Due to the horizontal plane of mirror symmetry of the array, the underlying resonant mode has a certain parity and has coupled to the two channels with symmetric radiative decay rates. Correspondingly, the non-resonant background can be assumed to be nearly transparent, $r_C \approx 0$, consistent with transparency of the array away from its resonant frequency (but still away from diffraction). For such an arrangement, one can show analytically that the system becomes fully reflective at its resonance. Non-zero reflective background, $r_C \neq 0$, shifts the spectral position of the reflection maximum, but it still reaches exactly 1 at the Fano resonance of the system [50, 52].

4. FINITE-SIZE ARRAY

Now we move to to a system containing a finite number of rods. Consider an array of N scatterers described by point sources located at $\mathbf{r}_1, \mathbf{r}_2, ..., \mathbf{r}_N$. Here, we utilize the original Foldy-Lax formulation of scattering problem in the coupled dipole approximation similar to Eq. (8):

$$\mathbf{E}^{\text{tot}}(\mathbf{r}) = \mathbf{E}^{\text{inc}}(\mathbf{r}) + 4\pi k_0^2 \sum_{j=1}^{N} G(\mathbf{r}, \mathbf{r}_j)\mathbf{P}(\mathbf{r}_j), \tag{23}$$

where $\mathbf{P}_j \equiv \mathbf{P}(\mathbf{r}_j) = \alpha_{yy}\mathbf{E}^{\text{tot}}(\mathbf{r}_j)$ is the dipole moment of the jth scatterer defined self-consistently by the exciting field, and G is the free space Green's function introduced earlier, Eq. (6). Once again, we will assume that the plane of incidence is perpendicular to the rods, i.e., $\mathbf{r} = (x, z)^{\text{T}}$ [see Fig. 2(a)]. As it follows from the relations (3), (7) and (11), for TM polarization only the y-component of dipole moments and electric field is required for further evaluations, so next we will operate with scalar quantities. Multiplying Eq. (23) by individual cylinder's

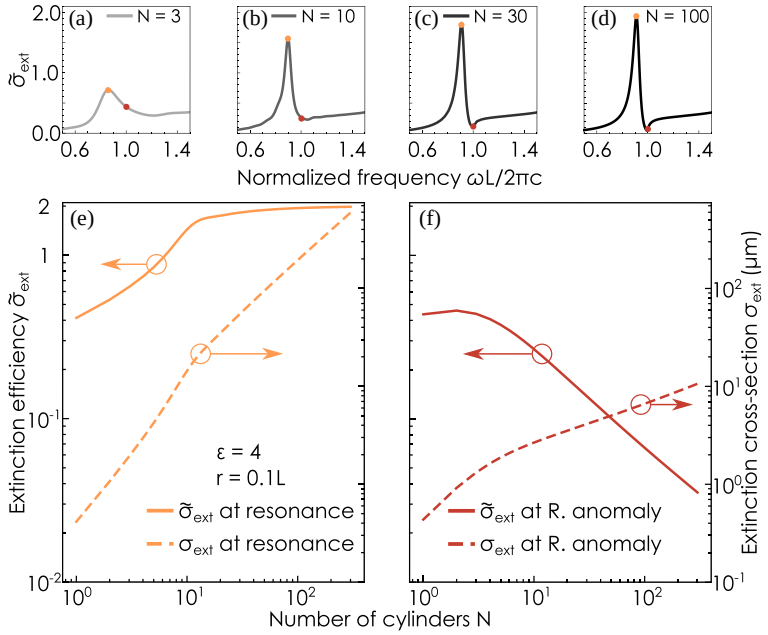

FIGURE 3. (a)–(d) Extinction efficiency spectra of finite periodic arrays of circular dielectric rods ($\varepsilon = 4$, $r = 0.1L$) for different number of rods $N = 3, 10, 30, 100$ under normally incident TM-polarized illumination. Orange dots mark the position of the lattice resonance, while the red dots mark the position of the Rayleigh frequency of the infinitely extended ($N = \infty$) structure. (e) Extinction cross-section (dashed) and extinction efficiency (solid) of a finite array of dielectric rods as functions of N evaluated with the CDA model at the lattice resonance. (f) Same as (e) but evaluated at the Rayleigh anomaly of the array.

polarizability α_{yy} and substituting $\mathbf{r} = \mathbf{r}_i$, we obtain a system of coupled linear equations:

$$P_i = \alpha_{yy}\mathcal{E}e^{ik_z z_i + ik_\parallel x_i} + 4\pi k_0^2 \alpha_{yy} \sum_{j\neq i} G(\mathbf{r}_i, \mathbf{r}_j) P_j, \quad (24)$$

where P_i is the y-component of $\mathbf{P}_j$. Rearranging the terms in this system, we rewrite it in a compact matrix form:

$$\overleftrightarrow{\mathbf{M}}(\omega)\mathbb{P} = \mathbb{E}^{\text{inc}}, \quad (25)$$

where $\mathbb{P}$ and $\mathbb{E}^{\text{inc}}$ denote the super-vectors of dipole moments and incident fields:

$$\mathbb{P} = \begin{pmatrix} P_1 \\ \vdots \\ P_N \end{pmatrix}, \quad \mathbb{E}^{\text{inc}} = \begin{pmatrix} E_y^{\text{inc}}(\mathbf{r}_1) \\ \vdots \\ E_y^{\text{inc}}(\mathbf{r}_N) \end{pmatrix} = \mathcal{E} \begin{pmatrix} e^{ik_z z_1 + ik_\parallel x_1} \\ \vdots \\ e^{ik_z z_N + ik_\parallel x_N} \end{pmatrix}, \quad (26)$$

and $\overleftrightarrow{\mathbf{M}}$ is the coupling matrix:

$$\overleftrightarrow{\mathbf{M}}(\omega) = \alpha_{yy}^{-1}\overleftrightarrow{\mathbb{I}} - 4\pi k_0^2 \times \begin{pmatrix} 0 & G(\mathbf{r}_1, \mathbf{r}_2; \omega) & \cdots & G(\mathbf{r}_1, \mathbf{r}_N; \omega) \\ G(\mathbf{r}_2, \mathbf{r}_1; \omega) & 0 & \cdots & G(\mathbf{r}_2, \mathbf{r}_N; \omega) \\ \vdots & & \ddots & \vdots \\ G(\mathbf{r}_N, \mathbf{r}_1; \omega) & G(\mathbf{r}_N, \mathbf{r}_2; \omega) & \cdots & 0 \end{pmatrix}. \quad (27)$$

Resolving Eq. (25) with respect to the dipole moments, we obtain:

$$\mathbb{P} = \overleftrightarrow{\mathbf{M}}^{-1}(\omega)\mathbb{E}^{\text{inc}}, \quad (28)$$

which formally expresses the solution of the coupled dipoles problem. In general, the coupling matrix is not guaranteed to be invertible at every frequency ω. In particular, it might not be invertible at a bound state in the continuum. That, however, would require an infinite system $N = \infty$.

The dipole moment values obtained from Eq. (28) yield the extinction cross-section of the finite system:

$$\sigma_{\text{ext}} = \frac{4\pi k_0}{|\mathcal{E}|^2} \sum_{i=1}^{N} \Im\text{m}\left[P_i^* E^{\text{inc}}(\mathbf{r}_i)\right]. \quad (29)$$

Finally, we introduce the extinction efficiency defined as:

$$\tilde{\sigma}_{\text{ext}} = \frac{\sigma_{\text{ext}}}{NL}. \quad (30)$$

Figures 3(a)–(d) show a series of extinction efficiency spectra for finite arrays with different numbers N of subwavelength dielectric cylinders illuminated with a normally incident TE-polarized plane wave. While for a single cylinder, $N = 1$, the extinction efficiency expectedly does not feature any resonant effects, sharp peaks and dips associated with the lattice resonances (orange dots) and Rayleigh anomalies (red dots) gradually appear for larger N. Extinction efficiency evaluated at the lattice resonance frequency rapidly approaches 2 with growing N, Fig. 3(e). Section S1 of Supplemental Material contains a

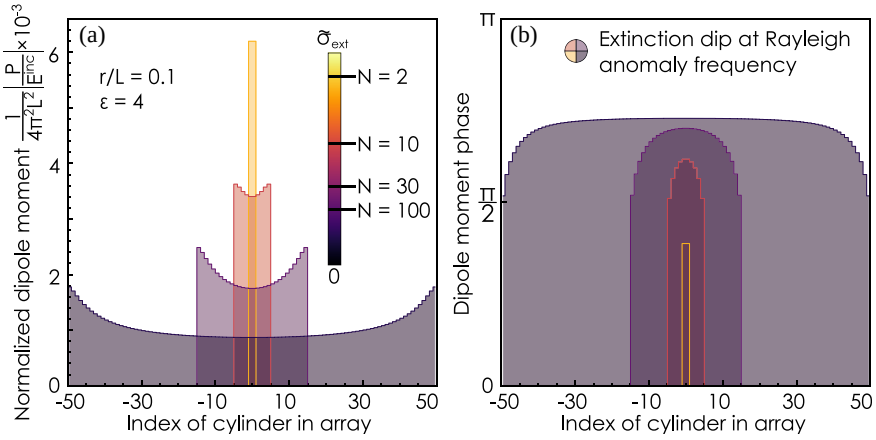

FIGURE 4. Spatial distribution of the normalized induced dipole moment absolute values $|P_i|$ (a) and dipole moment arguments $\arg P_i$ (b) in finite arrays of dielectric rods ($\varepsilon = 4$, $r = 0.1L$) obtained with the CDA model for $N = 2, 10, 30, 100$ at the frequency of Rayleigh anomaly of infinite system. The color of each plot encodes the extinction efficiency of the system , see the color bar in the inset.

more detailed discussion of complex-valued resonant frequencies of finite arrays and their evolution with N.

Conversely, at the first Rayleigh frequency, $\omega L/2\pi c = 1$, the absolute extinction still grows with N, but the extinction efficiency vanishes in the limit of infinite array, $N \to \infty$. Thus, at the Rayleigh anomaly the system becomes more transparent in terms of extinction efficiency with increasing number of scattering elements. More precisely, the extinction efficiency scales asymptotically as $\tilde{\sigma}_{\text{ext}} \propto 1/\sqrt{N}$ [see Fig. 3(f)]. Such a slow convergence to the value predicted for an infinite system is caused by the lattice sum representing a conditionally convergent series of Hankel functions.

It is known that per-unit-area extinction σ/A of a truly infinite periodic metasurface can be expressed as [53]

$$\sigma/A = 2\mathfrak{Re}(1-t), \tag{31}$$

where t is the complex-valued zero-order (specular) transmission amplitude of the periodic system.

Exactly at the Rayleigh anomaly $t = 1$ (see Fig. S3 for the plot of complex-valued transmission amplitude t), thus yielding $\sigma/A = 0$. This corresponds to the incident field performing no net work on the induced currents whatsoever, consistent with near-ideal transparency.

A more peculiar situation occurs at the lattice resonance frequency. Plugging $t = 0$ in (31) one obtains $\sigma/A = 2$, which is exactly the result we observe in the extinction efficiency of large finite arrays at the lattice resonance, Fig. 3(e). This reminds the situation with the extinction paradox, wherein scattering cross-section of a perfectly conducting sphere in the limit of short wavelength is twice of its geometric cross-section [54].

To provide more insight into the total transmission effect at the Rayleigh anomaly, we analyze the distribution of the induced dipole moments along the finite array upon a monochromatic TM-polarized illumination at the Rayleigh frequency $\omega L/2\pi c = 1$. Fig. 4 shows the magnitude of the induced dipole moments of the dielectric cylinders as a function of the cylinder index for a series of N values. Clearly, the magnitudes drop in every section of the array with increasing total number of elements N. Furthermore, one can clearly notice the edge effect: for any given N the dipole moments magnitude grows towards the edge, which is due to the uncompensated field from the missing dipoles at the edge of the array [Fig. 4(a)].

In addition, at the Rayleigh anomaly dipole moments phases possess the similar behavior — the argument of each dipole moment with growing N tends to π thus minimizing $\mathfrak{Im}[P_i]$. Thus, infinitely large array $N \longrightarrow \infty$ becomes fully "transparent". However, the dipoles at the edges still provide a significant contribution to extinction due to $\arg P_{\pm N/2} \longrightarrow \pi/2$, making corresponding large dipole moment purely imaginary [Fig. 4(b)]. Section S2 of Supporting Information offers more analysis of the per-dipole extinction convergence.

In the limit $N \to \infty$, the edge effect would disappear, and the induced dipole moments get totally suppressed at the Rayleigh anomaly leading to total transparency of the array. It is worth noting that the presented mechanism of total transparency relies on the inter-particle interaction within the array and differs from the effects in individual particles, such as anapole [55] or Kerker effect [56] based on the destructive interference of certain multipole moments in backward direction.

4.1. The Effect of Material Absorption

The previous analysis ignores possible absorption in dielectric cylinders. It is instructive now to examine how the presence of dissipation affects the results in light of the results on infinite arrays, which predict the transparency of the periodic system at the Rayleigh anomaly even in the presence of material loss [1]. By introducing material loss, we have to distinguish contributions from absorption and scattering to the extinction cross-section. Absorption efficiency can be defined similarly to extinction efficiency, Eq. (30), by replacing the background field with the total one [57]:

$$\tilde{\sigma}_{\text{abs}} = \frac{4\pi k_0}{NL|\mathcal{E}|^2} \sum_{i=1}^{N} \mathfrak{Im}\left[P_i^* \cdot E^{\text{tot}}(\mathbf{r}_i)\right]. \tag{32}$$

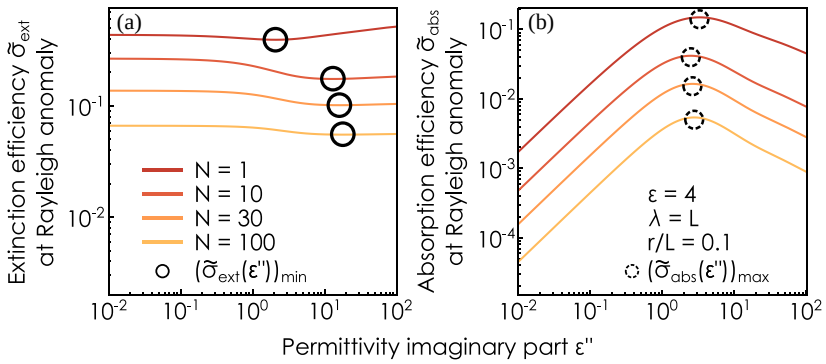

FIGURE 5. Extinction efficiency $\tilde{\sigma}_{\text{ext}}$ (a) and absorption efficiency $\tilde{\sigma}_{\text{abs}}$ (b) for finite periodic arrays ($\text{Re}\{\varepsilon\} = 4$, $r = 0.1L$) with fixed number of rods under TM-polarized illumination at the Rayleigh frequency ($\omega L/2\pi c = 1$) as a function of the imaginary part of the permittivity $\Im\text{m}[\varepsilon] = \varepsilon''$. Solid circles show extinction minima and dashed circles show the absorption maxima.

Figure 5 presents the resulting extinction $\tilde{\sigma}_{\text{ext}}$ and absorption $\tilde{\sigma}_{\text{abs}}$ efficiencies as a function of the imaginary part of the cylinders permittivity ε'' at the Rayleigh wavelength for a series of N. For each N the absorption efficiency reaches a maximum at a certain value of ε'', Fig. 5(b).

At the same time, the increase of ε'' suppresses the extinction efficiency below the initial value until it reaches a minimum, and then starts to increase approaching an asymptotic value, Fig. 5(a). The results in Fig. 5(a) are rather counterintuitive. An array of lossless cylinders becomes transparent at the Rayleigh anomaly in the limit of infinite array, $N \to \infty$ [see Fig. 2(c)]. A non-scattering optical system, such as an anapole nanodisk or an array of those, starts to scatter *more* with increasing material dissipation in agreement with the optical theorem [58, 59]. Nevertheless, increasing material absorption of the cylinders further suppresses extinction until the minimum value is reached.

The behavior shown in Fig. 5(b) is reminiscent of the critical coupling phenomenon [60]. Critical coupling describes the behavior of a single-mode optical structure coupled radiatively at a rate γ_{rad} to a single scattering channel, and at the same time experiencing a non-radiative decay at a rate $\gamma_{\text{non-rad}}$. Given balanced decay rates, $\gamma_{\text{rad}} = \gamma_{\text{non-rad}}$, the system exhibits ideal absorption upon illumination from that scattering channel. For a spherically (cylindrically) symmetric object critical coupling requires illumination with an appropriate vector spherical (cylindrical) harmonic. A plane wave illumination then manifests as maximized and equal partial absorption and scattering cross-sections into that particular multipolar channel [58, 59, 61]. However, the fundamental lattice resonance of our finite system of $N \gg 1$ rods is coupled to a great number of multipolar scattering channels. This complicated structure of the lattice resonance hinders the observation of either perfect absorption or equalized partial cross-sections. Nevertheless, the maxima of the total absorption cross-section observed at specific values of $\Im\text{m}\varepsilon$ strongly suggest that the finite system becomes critically coupled at that point, but requires a complicated incoming wave front for the observation of critical coupling.

It is worth mentioning that the absorptive performance of the system is entirely due to the properties of the individual particles, since the matrix denominator in (12) contains factors consisting of two terms groups. While the second group describing array properties does not change with the material losses, the first one, represented through the inverse polarizability, determines the absorbing properties.

The inverse polarizability of a 2D scatterer takes the following form in quasi-static limit:

$$\alpha_{yy}^{-1} = \xi' + \text{i}\xi'' + \frac{\text{i}}{4}\, k_0^2, \tag{33}$$

where ξ' is the electrostatic term; ξ'' represents absorption; and the last term describes the radiation correction [58]. Utilizing the Taylor series expansion of b_0 (2) at $k_0 r \to 0$, one can notice that ξ'' vanishes in the limit of both small and very large material losses. As a result, in both limits the dominant contribution to the extinction efficiency is provided by scattering cross-section. Indeed, $\sigma_{\text{abs}} \propto \varepsilon''$ in the limit $\varepsilon'' \ll 1$, and $\sigma_{\text{abs}} \propto 1/\sqrt{\varepsilon''}$ in the limit $\varepsilon'' \gg 1$, according to results shown in Fig. 5(b).

4.2. Finite-Size Metallic Arrays

To further demonstrate the universal nature of the collective transparency at the Rayleigh anomaly, we also confirm its occurrence in a finite array of *metallic* circular rods described by lossless Drude model, $\varepsilon(\omega) = 1 - \omega_p^2/\omega^2$, where ω_p is plasma frequency. The CDA model developed above remains fully valid as long as one adjusts the cylinders polarizability α_{yy} accounting for frequency-dependent Drude permittivity.

Figures 6(a)–(c) present reflection spectra of infinite periodic arrays of metallic rods with different ratios L/λ_p encoding the strength of metallic response. Clearly, the array of thin metallic cylinders becomes perfectly reflective in the low-frequency limit. Still, the lattice sum G_{latt} diverges exactly at the same Rayleigh anomaly, rendering the array of metallic rods fully transparent upon TM-polarized illumination at each Rayleigh anomaly, Figs. 6(a)–(c).

In finite arrays of metallic cylinders with relatively small plasma frequency, $L/\lambda_p < 1$, the drop of normalized extinc-

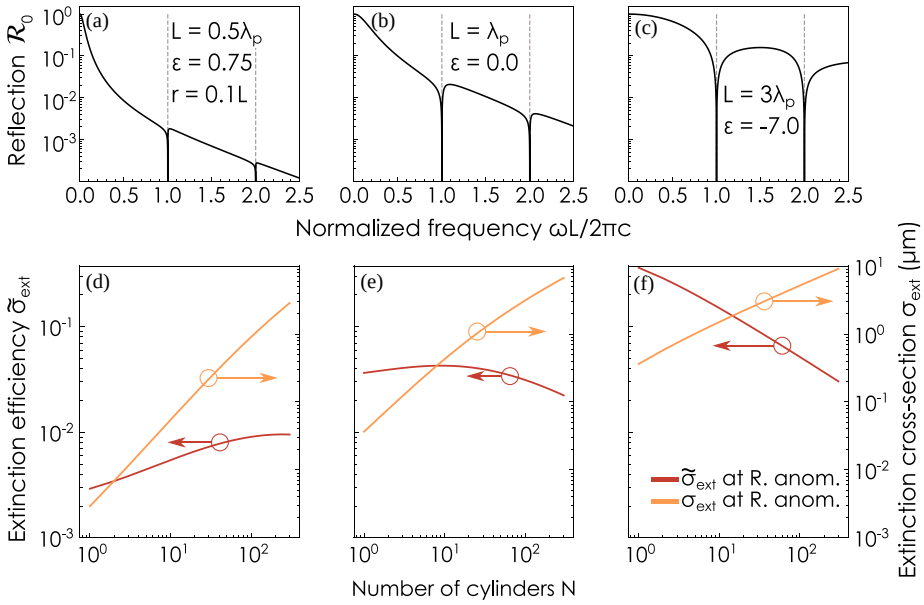

FIGURE 6. (a)–(c) Specular reflection spectra of infinite periodic arrays of circular Drude rods ($r = 0.1L$) for different plasma wavelengths under normally incident TM-polarized illumination. Grey dashed lines mark the Rayleigh anomaly frequencies. ε indicate the value of the rod's permittivity at the first Rayleigh anomaly, $\omega L/2\pi c = 1$. (d)–(f) Extinction cross-section (orange) and extinction efficiency (red) of a finite array of Drude rods as functions of on N obtained with the CDA model at the first Rayleigh anomaly frequency $\omega L/2\pi c = 1$ for different plasma wavelengths $\lambda_p/L = 2, 1, 1/3$, respectively.

tion does not occur until a large number of scatterers N is involved, Fig. 6(d). In arrays of cylinders with more pronounced metallic properties, $L/\lambda_p \geq 1$; on the other hand, the drop of normalized extinction occurs at much smaller number of cylinders, Figs. 6(e) and (f).

5. NUMERICAL SIMULATIONS: CIRCULAR CROSS-SECTION

Next, we verify the validity of the CDA model used above. To that end we perform a series of full-wave numerical simulations for $N = 30$ cylinders of different sizes in COMSOL Multiphysics. To that end, we calculate the scattering cross-section by integrating the energy flux over the boundary ∂V between the Perfectly Matched Layers and cylinders as

$$\sigma_{\text{sct}} = \frac{1}{2I^{\text{inc}}} \oint_{\partial V} \Re\text{e}\left[\mathbf{E}^{\text{sct}} \times (\mathbf{H}^{\text{sct}})^*\right] \cdot \mathbf{n} dS, \qquad (34)$$

where I^{inc} is the energy flux of the incident field. The absorption cross-section was obtained by the integration over scatterers domain V by the following expression:

$$\sigma_{\text{abs}} = \frac{1}{2I^{\text{inc}}} \int_V \Re\text{e}\left[\mathbf{j} \cdot (\mathbf{E}^{\text{tot}})^*\right] dV, \qquad (35)$$

where $\mathbf{j}$ is the total current density induced by total field $\mathbf{E}^{\text{tot}}$. Finally, extinction cross-section was determined as the sum of the absorption and scattering cross-sections, $\sigma_{\text{ext}} = \sigma_{\text{sct}} + \sigma_{\text{abs}}$.

For small cylinders ($r = 0.1L$), the resulting extinction efficiency spectra show a great agreement (with an accuracy of 10^{-2}) up to the first Rayleigh anomaly, $\omega L \leq 2\pi c$, Fig. 7(a). At the higher frequencies, the results predicted by the models begin to diverge. This discrepancy originates from the contributions of higher order multipole moments to the scattered field, which become particularly significant above the first Rayleigh anomaly. The magnitude of each contribution is proportional to the corresponding scattering coefficient a_l or b_l, $l = 0, 1, 2, \ldots$, which is in turn a function of dimensionless size parameter $\sqrt{\varepsilon} k_0 r$.

For thicker cylinders ($r = 0.25L$), the discrepancy between the CDA and numerical simulations appears even below the Rayleigh anomaly in the sub-diffraction regime, Fig. 7(d). The total transparency effect is no longer observed at the Rayleigh frequency or in its vicinity according to the results of numerical simulations (the orange curve in Fig. 7(d)). Instead, the array of thick cylinders in fact becomes nearly transparent at the point of a Fano resonance below the first diffraction threshold, Fig. S4. This is accompanied by the extinction efficiency approaching 4 at the resonance, Fig. 7(d).

Next, Figs. 7(b), (c), (e), and (f) illustrate the cross-sectional view of the total and scattered parts of the electric field at the Rayleigh anomaly in the vertical plane evaluated with the CDA model and the numerical simulations for $N = 30$ arrays of thin and thick circular cylinders. For thin cylinders ($r = 0.1L$), the CDA and numerical models show great agreement in evaluation of the total and scattered field. For thick cylinders ($r = 0.25L$), however, predictions of the CDA model clearly become incorrect at the Rayleigh anomaly. While the CDA model predicts the absence of radiated field and unperturbed transmission of the incident wave, which is clearly not the case in full-wave numerical simulations.

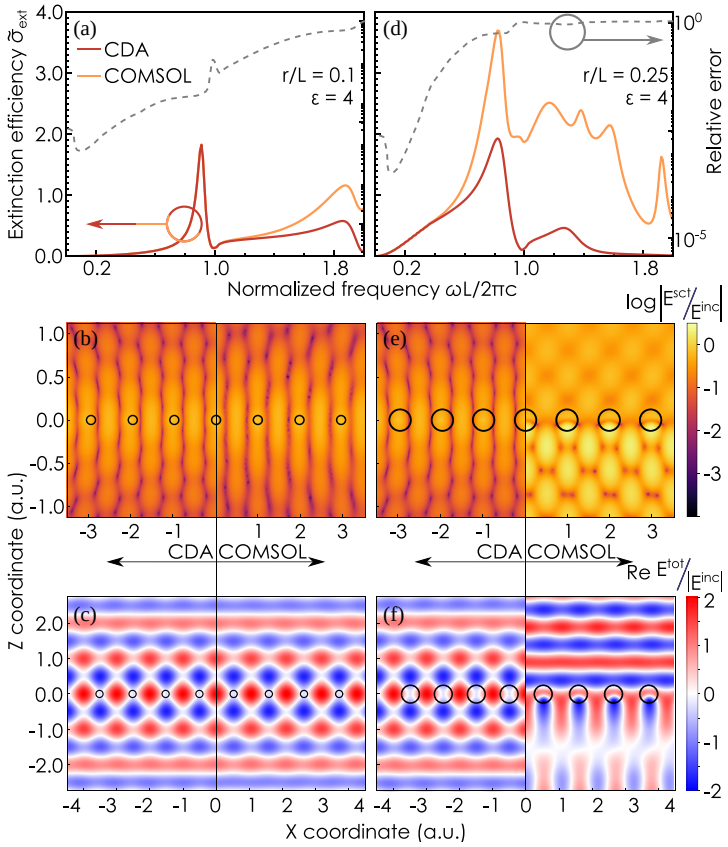

FIGURE 7. (a) Comparison of the extinction efficiency $\tilde{\sigma}_{\text{ext}}$ spectra obtained via the CDA model (red solid line) and via COMSOL Multyphysics numerical simulation (orange solid line) for a finite array of $N = 30$ circular cylinders ($\varepsilon = 4$, $r = 0.1L$). Dashed gray curve shows the relative error (log scale). (b) Cross-section view of the magnitude of the scattered electric field (log scale) and (c) real part of the total electric field in the plane orthogonal to the cylinders axis for $N = 30$, obtained with the CDA model (left part of the panel) and by COMSOL Multyphysics numerical simulations (right part of the panel) at the Rayleigh frequency. Black circles represent the scatterers sizes and positions. (d) – (f) Same as (a) – (c), respectively, but for thicker circular cylinders with $r = 0.25L$.

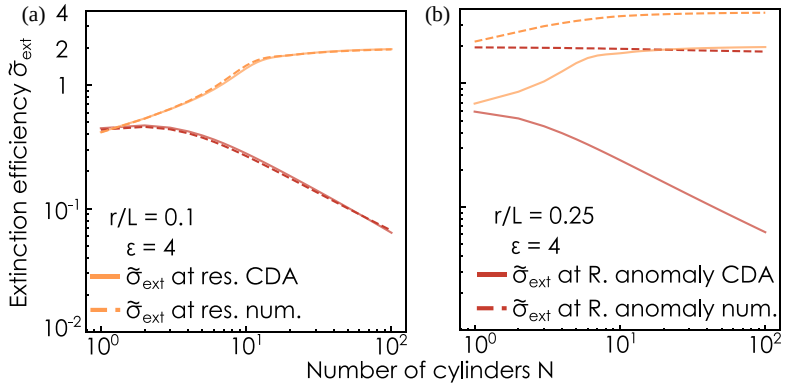

FIGURE 8. (a) Extinction efficiency obtained from analytics (solid) and numerical simulations (dashed) as functions of N for finite arrays of N dielectric cylinders ($\varepsilon = 4$, $r = 0.1L$) at the lattice resonance (orange) and at the Rayleigh anomaly (red). (b) same as (a) for thicker rods, $r = 0.25L$.

Figure 8 compares the behavior of the extinction efficiencies vs N obtained with the CDA model (Figs. 3(e) and (f)) to those obtained with numerical simulations for the two cases of interest (at the Rayleigh anomaly and at the resonance). In both scenarios, the relative error of the CDA model with respect to more exact numerical simulations stays on the level of a few percent, which suggests that we can keep using the CDA model for the evaluation of extinction efficiencies of the system for relatively thin dielectric cylinders, $r \leq 0.1L$. For thick circular rods, $r = 0.25L$, the relative error becomes much larger, clearly indicating that the CDA model is no longer valid.

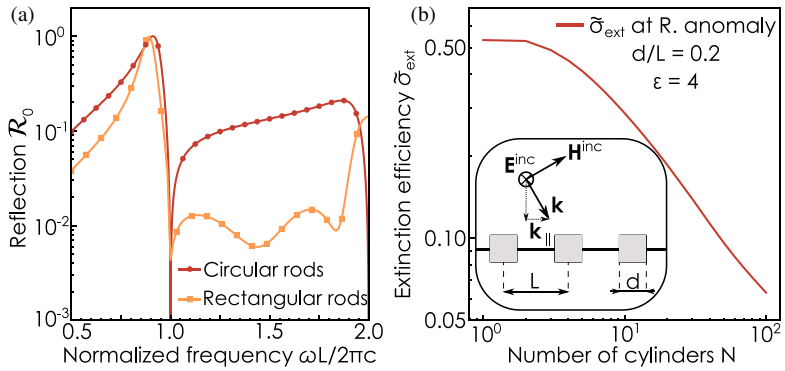

FIGURE 9. (a) Numerically simulated specular reflection $\mathfrak{R}_0$ spectra for infinite arrays of dielectric rods with circular and square cross-sections. Both arrays exhibit perfect transmission at the Rayleigh anomaly. (b) Extinction efficiency of a finite array of square rods evaluated at the Rayleigh anomaly as a function of N.

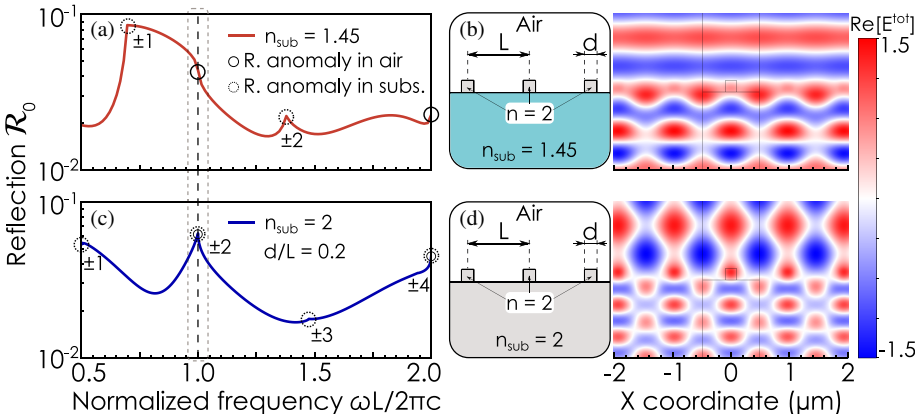

FIGURE 10. Numerical simulations: the effect of dielectric $n_{\text{sub}} = 1.45$ substrate for (a), (b) and $n_{\text{sub}} = 2$ substrate for (c), (d). As follows from the spectra in panels (a) and (c), the presence of a substrate violates the perfect transmission at Rayleigh anomalies of the arrays. (b) and (d) show normalized total field as function of the coordinates.

6. NUMERICAL SIMULATIONS: NON-CIRCULAR CROSS-SECTION AND THE EFFECT OF SUBSTRATE

Next, we move on to the analysis of analogous effects in realistic systems incorporating dielectric rods of square cross-section and possibly a dielectric substrate. To begin with, we analyze an infinite array of square rods and highlight the key differences from the case of circular cylinders. As one can see from Fig. 9(a), below the onset of diffraction, $\omega L/2\pi c < 1$, a periodic array of square (cross-section) rods features the intensity reflection similar to that of circular cylinders.

As long as the CDA model is valid, the analytical expressions for the response of the periodic array (Eqs. (15) and (16)) remain applicable to the arrays of square/rectangular rods with an appropriate bare polarizability α_{yy} in the denominator of Eq. (12) (which can be calculated numerically with a desired precision). The term G_{latt} corresponding to the effect of the lattice remains unchanged. Thus, the total transmission effect remains observed at the Rayleigh anomaly of the infinite periodic array at $\omega L/2\pi c = 1$. However, at higher frequencies, there are notable differences in the reflection spectra of circular and square rods. Those could be caused by the excitation of higher multipole moments in the array of square rods, which lead to a destructive interference and cause a substantially lower specular reflection of arrays of square rods, Fig. 9(a). As a result of the analytical equivalence mentioned above, the extinction efficiency of a finite array of square rods at the Rayleigh anomaly retains the same asymptotic behavior as a function of the number of the elements in the array N, Fig. 9(b).

Finally, we analyze how the presence of a dielectric substrate would affect the spectral features — in particular, the total transparency at the Rayleigh anomaly — of an infinite periodic array. Fig. 10(a) shows simulated intensity reflection spectrum of an array of square cross-section dielectric rods, with refractive index $n = 2$ and height $d = 0.2L$, lying on top of a quartz substrate, $n_{\text{sub}} = 1.45$ [see the geometry sketch in Fig. 10(b)]. As one can see, both the effects of total reflection at the lattice resonance and the total transmission at the Rayleigh anomaly $\omega L = 2\pi c$ are gone with the dielectric substrate present. These changes are mainly caused by the strong near-field interactions of the rods with the substrate, which, due to the vanishingly small distance between the dielectrics, turn out to be the most significant. For this particular configuration the reflection coefficient is rather small, but still a non-zero value around 0.05 at the Raleigh anomaly, Fig. 10(a). Correspondingly, this non-

zero reflection causes noticeable distortion of the total field calculated right at the Raleigh anomaly.

Another remarkable spectral feature is the occurrence of a sharp reflection peak at $\omega L/2\pi c \approx 1.4$. Counter-intuitively, this peak is not a resonant feature of the system, but instead is related to the onset of the $m = \pm 2$ diffraction order in the dielectric substrate, which is justified by noticing that corresponding Rayleigh anomaly for dielectric with $n_{\text{sub}} = 1.45$ is exactly at stated frequency. In contrast to the Rayleigh anomaly in free-standing arrays, this Rayleigh anomaly does not manifest itself as a reflection zero or a reflection dip [62].

A qualitatively similar picture is observed in the case of identical material of the scatterers and the substrate with $n_{\text{sub}} = n = 2$ [see Fig. 10(d)]. Since the substrate index is an integer multiple of the superstrate index, each even Rayleigh anomaly in the substrate matches a Rayleigh anomaly in air, Fig. 10(c). Similar to the previous case of a glass substrate, the total field at the Rayleigh anomaly is substantially distorted away from the background field, Fig. 10(d).

Including substrate in an experimental scenario would thus complicate, if not make impossible, the potential observation of perfect transparency at the Rayleigh anomaly. However, similar arrays have been fabricated using free-standing dielectric membranes in air [23]. This approach could allow experimental observation of the diffraction effects in finite arrays in a substrate-free configuration.

7. CONCLUSION

To conclude, we have theoretically and numerically studied the evolution of diffractive spectral features in finite arrays of subwavelength circular dielectric rods. The results of the coupled dipoles approximation-based analytical model indicate that finite arrays do become transparent at the Rayleigh anomaly in terms of the normalized extinction. This transition to transparency is accompanied by a gradual suppression of the induced dipole moments of the rods along the chain as the number of elements of the finite system increases. Furthermore, the presence of material absorption barely affects the transparency of finite arrays at the diffraction anomaly. Full-wave numerical simulations validate the results of the analytical model in the limit of subwavelength rods and suggest that these phenomena survive for non-circular cross-section of the rods. Finally, we show that the presence of a dielectric substrate will possibly destroy the effects of perfect transmission and the lattice resonance and finite and infinite arrays of subwavelength rods. Our results could provide more insights into the diffractive effects in finite periodic systems.

ACKNOWLEDGEMENT

D.G.B. acknowledges support from Russian Science Foundation (grant No. 23-72-10005) and BASIS Foundation (grant No. 22-1-3-2-1). I.K. and R.N. acknowledge support from Russian Science Foundation (grant No. 23-72-10059) and the Priority 2030 Federal Academic Leadership Program. The authors acknowledge the ITMO-MIPT-Skoltech Clover initiative.

REFERENCES

[1] De Abajo, F. J., "Colloquium: Light scattering by particle and hole arrays," *Reviews of Modern Physics*, Vol. 79, No. 4, 1267–1290, 2007.

[2] Ebbesen, T. W., H. J. Lezec, H. F. Ghaemi, T. Thio, and P. A. Wolff, "Extraordinary optical transmission through subwavelength hole arrays," *Nature*, Vol. 391, No. 6668, 667–669, 1998.

[3] Martín-Moreno, L., F. J. García-Vidal, H. J. Lezec, K. M. Pellerin, T. Thio, J. B. Pendry, and T. W. Ebbesen, "Theory of extraordinary optical transmission through subwavelength hole arrays," *Physical Review Letters*, Vol. 86, No. 6, 1114, 2001.

[4] Silveirinha, M. G., P. A. Belov, and C. R. Simovski, "Subwavelength imaging at infrared frequencies using an array of metallic nanorods," *Physical Review B — Condensed Matter and Materials Physics*, Vol. 75, No. 3, 035108, 2007.

[5] Ono, A., J.-I. Kato, and S. Kawata, "Subwavelength optical imaging through a metallic nanorod array," *Physical Review Letters*, Vol. 95, No. 26, 267407, 2005.

[6] Rayleigh, L., "III. Note on the remarkable case of diffraction spectra described by Prof. Wood," *The London, Edinburgh, and Dublin Philosophical Magazine and Journal of Science*, Vol. 14, No. 79, 60–65, 1907.

[7] Wood, R. W., "XLII. On a remarkable case of uneven distribution of light in a diffraction grating spectrum," *The London, Edinburgh, and Dublin Philosophical Magazine and Journal of Science*, Vol. 4, No. 21, 396–402, 1902.

[8] Auguié, B. and W. L. Barnes, "Collective resonances in gold nanoparticle arrays," *Physical Review Letters*, Vol. 101, No. 14, 143902, 2008.

[9] Manjavacas, A., L. Zundel, and S. Sanders, "Analysis of the limits of the near-field produced by nanoparticle arrays," *ACS Nano*, Vol. 13, No. 9, 10 682–10 693, 2019.

[10] Marinica, D. C., A. G. Borisov, and S. V. Shabanov, "Bound states in the continuum in photonics," *Physical Review Letters*, Vol. 100, No. 18, 183902, 2008.

[11] Zhen, B., C. W. Hsu, L. Lu, A. D. Stone, and M. Soljačić, "Topological nature of optical bound states in the continuum," *Physical Review Letters*, Vol. 113, No. 25, 257401, 2014.

[12] Koshelev, K. L., Z. F. Sadrieva, A. A. Shcherbakov, Y. S. Kivshar, and A. A. Bogdanov, "Bound states in the continuum in photonic structures," *Phys.-USP*, Vol. 93, 528–553, 2023.

[13] Joseph, S., S. Pandey, S. Sarkar, and J. Joseph, "Bound states in the continuum in resonant nanostructures: An overview of engineered materials for tailored applications," *Nanophotonics*, Vol. 10, No. 17, 4175–4207, 2021.

[14] Maslova, E. E., M. V. Rybin, A. A. Bogdanov, and Z. F. Sadrieva, "Bound states in the continuum in periodic structures with structural disorder," *Nanophotonics*, Vol. 10, No. 17, 4313–4321, 2021.

[15] Kang, M., L. Mao, S. Zhang, M. Xiao, H. Xu, and C. T. Chan, "Merging bound states in the continuum by harnessing higher-order topological charges," *Light: Science & Applications*, Vol. 11, No. 1, 228, 2022.

[16] Hwang, M.-S., K.-Y. Jeong, J.-P. So, K.-H. Kim, and H.-G. Park, "Nanophotonic nonlinear and laser devices exploiting bound states in the continuum," *Communications Physics*, Vol. 5, No. 1, 106, 2022.

[17] Kang, M., T. Liu, C. T. Chan, and M. Xiao, "Applications of bound states in the continuum in photonics," *Nature Reviews Physics*, Vol. 5, No. 11, 659–678, 2023.

[18] Gomez-Medina, R., M. Laroche, and J. J. Sáenz, "Extraordinary optical reflection from sub-wavelength cylinder arrays," *Optics Express*, Vol. 14, No. 9, 3730–3737, 2006.

[19] Borisov, A. G., F. J. G. d. Abajo, and S. V. Shabanov, "Role of electromagnetic trapped modes in extraordinary transmission in nanostructured materials," *Physical Review B*, Vol. 71, No. 7, 075408, 2005.

[20] Laroche, M., S. Albaladejo, R. Gómez-Medina, and J. J. Sáenz, "Tuning the optical response of nanocylinder arrays: An analytical study," *Physical Review B*, Vol. 74, No. 24, 245422, 2006.

[21] Laroche, M., S. Albaladejo, R. Carminati, and J. J. Sáenz, "Optical resonances in one-dimensional dielectric nanorod arrays: Field-induced fluorescence enhancement," *Optics Letters*, Vol. 32, No. 18, 2762–2764, 2007.

[22] Du, J., Z. Lin, S. T. Chui, G. Dong, and W. Zhang, "Nearly total omnidirectional reflection by a single layer of nanorods," *Physical Review Letters*, Vol. 110, No. 16, 163902, 2013.

[23] Ghenuche, P., G. Vincent, M. Laroche, N. Bardou, R. Haïdar, J.-L. Pelouard, and S. Collin, "Optical extinction in a single layer of nanorods," *Physical Review Letters*, Vol. 109, No. 14, 143903, 2012.

[24] Evlyukhin, A. B., C. Reinhardt, A. Seidel, B. S. Luk'yanchuk, and B. N. Chichkov, "Optical response features of Si-nanoparticle arrays," *Physical Review B*, Vol. 82, No. 4, 045404, 2010.

[25] Evlyukhin, A. B., C. Reinhardt, U. Zywietz, and B. N. Chichkov, "Collective resonances in metal nanoparticle arrays with dipole-quadrupole interactions," *Physical Review B*, Vol. 85, No. 24, 245411, 2012.

[26] Zundel, L. and A. Manjavacas, "Finite-size effects on periodic arrays of nanostructures," *Journal of Physics: Photonics*, Vol. 1, No. 1, 015004, 2018.

[27] Sung, J., E. M. Hicks, R. P. V. Duyne, and K. G. Spears, "Nanoparticle spectroscopy: Plasmon coupling in finite-sized two-dimensional arrays of cylindrical silver nanoparticles," *The Journal of Physical Chemistry C*, Vol. 112, No. 11, 4091–4096, 2008.

[28] Zakomirnyi, V. I., A. E. Ershov, V. S. Gerasimov, S. V. Karpov, H. Agren, and I. L. Rasskazov, "Collective lattice resonances in arrays of dielectric nanoparticles: A matter of size," *Optics Letters*, Vol. 44, No. 23, 5743–5746, 2019.

[29] Karimi, V. and V. E. Babicheva, "Dipole-lattice nanoparticle resonances in finite arrays," *Optics Express*, Vol. 31, No. 10, 16 857–16 871, 2023.

[30] Schokker, A. H. and A. F. Koenderink, "Statistics of randomized plasmonic lattice lasers," *ACS Photonics*, Vol. 2, No. 9, 1289–1297, 2015.

[31] Hakala, T. K., H. T. Rekola, A. I. Väkeväinen, J.-P. Martikainen, M. Nečada, A. J. Moilanen, and P. Törmä, "Lasing in dark and bright modes of a finite-sized plasmonic lattice," *Nature Communications*, Vol. 8, No. 1, 13687, 2017.

[32] Wang, D., M. R. Bourgeois, J. Guan, A. K. Fumani, G. C. Schatz, and T. W. Odom, "Lasing from finite plasmonic nanoparticle lattices," *ACS Photonics*, Vol. 7, No. 3, 630–636, 2020.

[33] Ustimenko, N., C. Rockstuhl, and A. B. Evlyukhin, "Resonances in finite-size all-dielectric metasurfaces for light trapping and propagation control," *Physical Review B*, Vol. 109, No. 11, 115436, 2024.

[34] Hoang, T. X., D. Leykam, H.-S. Chu, C. E. Png, F. J. García-Vidal, and Y. S. Kivshar, "Collective nature of high-Q resonances in finite-size photonic metastructures," *arXiv preprint arXiv:2405.01034*, 2024.

[35] Volkov, I. A., N. A. Ustimenko, D. F. Kornovan, A. S. Sheremet, R. S. Savelev, and M. I. Petrov, "Strongly subradiant states in planar atomic arrays," *Nanophotonics*, Vol. 13, No. 3, 289–298, 2024.

[36] Volkov, I., S. Mitsai, S. Zhogolev, D. Kornovan, A. Sheremet, R. Savelev, and M. Petrov, "Non-radiative configurations of a few quantum emitters ensembles: Evolutionary optimization approach," *Applied Physics Letters*, Vol. 124, No. 8, 084001, 2024.

[37] Rui, J., D. Wei, A. Rubio-Abadal, S. Hollerith, J. Zeiher, D. M. Stamper-Kurn, C. Gross, and I. Bloch, "A subradiant optical mirror formed by a single structured atomic layer," *Nature*, Vol. 583, No. 7816, 369–374, 2020.

[38] Natarov, D. M., V. O. Byelobrov, R. Sauleau, T. M. Benson, and A. I. Nosich, "Periodicity-induced effects in the scattering and absorption of light by infinite and finite gratings of circular silver nanowires," *Optics Express*, Vol. 19, No. 22, 22 176–22 190, 2011.

[39] Natarov, D. M., R. Sauleau, M. Marciniak, and A. I. Nosich, "Effect of periodicity in the resonant scattering of light by finite sparse configurations of many silver nanowires," *Plasmonics*, Vol. 9, 389–407, 2014.

[40] Shapoval, O. V. and A. I. Nosich, "Finite gratings of many thin silver nanostrips: Optical resonances and role of periodicity," *AIP Advances*, Vol. 3, No. 4, 042120, 2013.

[41] Wei, Q.-H., K.-H. Su, S. Durant, and X. Zhang, "Plasmon resonance of finite one-dimensional Au nanoparticle chains," *Nano Letters*, Vol. 4, No. 6, 1067–1071, 2004.

[42] Linton, C. M. and P. A. Martin, "Semi-infinite arrays of isotropic point scatterers. A unified approach," *SIAM Journal on Applied Mathematics*, Vol. 64, No. 3, 1035–1056, 2004.

[43] Citrin, D. S., "Plasmon polaritons in finite-length metal-nanoparticle chains: The role of chain length unravelled," *Nano Letters*, Vol. 5, No. 5, 985–989, 2005.

[44] Hadad, Y. and B. Z. Steinberg, "Green's function theory for infinite and semi-infinite particle chains," *Physical Review B*, Vol. 84, No. 12, 125402, 2011.

[45] Savelev, R. S., D. S. Filonov, M. I. Petrov, A. E. Krasnok, P. A. Belov, and Y. S. Kivshar, "Resonant transmission of light in chains of high-index dielectric particles," *Physical Review B*, Vol. 92, No. 15, 155415, 2015.

[46] Kornovan, D. F., R. S. Savelev, Y. Kivshar, and M. I. Petrov, "High-Q localized states in finite arrays of subwavelength resonators," *ACS Photonics*, Vol. 8, No. 12, 3627–3632, 2021.

[47] Michaeli, L., O. Doron, Y. Hadad, H. Suchowski, and T. Ellenbogen, "Rayleigh anomaly induced phase gradients in finite nanoparticle chains," *Nanoscale*, Vol. 15, No. 33, 13 653–13 665, 2023.

[48] Hulst, H. C. and H. C. van de Hulst, *Light Scattering by Small Particles*, Courier Corporation, 1981.

[49] Markel, V. A., "Divergence of dipole sums and the nature of non-Lorentzian exponentially narrow resonances in one-dimensional periodic arrays of nanospheres," *Journal of Physics B: Atomic, Molecular and Optical Physics*, Vol. 38, No. 7, L115, 2005.

[50] Fan, S., W. Suh, and J. D. Joannopoulos, "Temporal coupled-mode theory for the Fano resonance in optical resonators," *Journal of the Optical Society of America A*, Vol. 20, No. 3, 569–572, 2003.

[51] Wang, K. X., Z. Yu, S. Sandhu, and S. Fan, "Fundamental bounds on decay rates in asymmetric single-mode optical resonators," *Optics Letters*, Vol. 38, No. 2, 100–102, 2013.

[52] Blanchard, C., J.-P. Hugonin, and C. Sauvan, "Fano resonances in photonic crystal slabs near optical bound states in the continuum," *Physical Review B*, Vol. 94, No. 15, 155303, 2016.

[53] Gustafsson, M., I. Vakili, S. E. B. Keskin, D. Sjoberg, and C. Larsson, "Optical theorem and forward scattering sum rule for periodic structures," *IEEE Transactions on Antennas and Propagation*, Vol. 60, No. 8, 3818–3826, 2012.

[54] Berg, M. J., C. M. Sorensen, and A. Chakrabarti, "A new explanation of the extinction paradox," *Journal of Quantitative Spectroscopy and Radiative Transfer*, Vol. 112, No. 7, 1170–1181, 2011.

[55] Miroshnichenko, A. E., A. B. Evlyukhin, Y. F. Yu, R. M. Bakker, A. Chipouline, A. I. Kuznetsov, B. Luk'yanchuk, B. N. Chichkov, and Y. S. Kivshar, "Nonradiating anapole modes in dielectric nanoparticles," *Nature Communications*, Vol. 6, No. 1, 8069, 2015.

[56] Kerker, M., D.-S. Wang, and C. L. Giles, "Electromagnetic scattering by magnetic spheres," *Journal of the Optical Society of America*, Vol. 73, No. 6, 765–767, 1983.

[57] Markel, V. A., "Antisymmetrical optical states," *Journal of the Optical Society of America B*, Vol. 12, No. 10, 1783–1791, 1995.

[58] Tretyakov, S., "Maximizing absorption and scattering by dipole particles," *Plasmonics*, Vol. 9, No. 4, 935–944, 2014.

[59] Fleury, R., J. Soric, and A. Alù, "Physical bounds on absorption and scattering for cloaked sensors," *Physical Review B*, Vol. 89, No. 4, 045122, Jan. 2014.

[60] Yariv, A., "Critical coupling and its control in optical waveguide-ring resonator systems," *IEEE Photonics Technology Letters*, Vol. 14, No. 4, 483–485, 2002.

[61] Mohammadi Estakhri, N. and A. Alù, "Minimum-scattering superabsorbers," *Physical Review B*, Vol. 89, No. 12, 121416, Mar. 2014.

[62] Auguié, B., X. M. Bendaña, W. L. Barnes, and F. J. G. de Abajo, "Diffractive arrays of gold nanoparticles near an interface: Critical role of the substrate," *Physical Review B*, Vol. 82, No. 15, 155447, 2010.